Supplementary material

Data preprocessing

a) ENIGMA data: Imaging data were processed by each center through the standard ENIGMA workflow. In brief, individual surface modeling was performed using FreeSurfer 5.3.0 [1–4], including magnetic field inhomogeneity correction, non-brain tissue removal, intensity normalization, and segmentation. White and pial surfaces were fit along tissue boundaries. Surfaces were inflated to spheres, followed by spherical registration to standard (fsaverage) space. Based on the Desikan-Killiany atlas [5], cortical thickness was measured across 68 grey matter brain regions.

b) HCP data: HCP data underwent minimal preprocessing pipelines using FSL, FreeSurfer, and Workbench, briefly summarized as follows [2,6,7]:

b-i) T1- and T2-weighted data: Data were corrected for gradient nonlinearity and b0 distortions, and the T1- and T2-weighted data were co-registered using a rigid-body transformation. The bias field was adjusted using the inverse intensities from the T1- and T2-weighting. White and pial surfaces were generated using FreeSurfer [1–4]. A midthickness surface was generated by averaging white and pial surfaces, and used to generate the inflated surface that was registered to the Conte69 template [8] using MSMAll [9] and downsampled to a 32k vertex mesh.

b-ii) Microstructure data: HCP provides a myelin-sensitive proxy based on the ratio of the T1- and T2-weighted contrast [10,11]. Here, we first generated 14 equivolumetric cortical surfaces within the cortex and sampled T1w/T2w ratio values along these surfaces [12]. A microstructural similarity matrix was constructed by calculating linear correlations of cortical depth-dependent T1w/T2w intensity profiles between different Desikan-Killiany parcels [5], controlling for the average whole-cortex intensity profile [12]. The matrix was thresholded at zero and log-transformed [12]. A group-average matrix was constructed by averaging matrices across participants.

b-iii) rs-fMRI data: Data were corrected for distortions and head motion, and were registered to the T1-weighted data and subsequently to MNI152 space. Magnetic field bias correction, skull removal, and intensity normalization were performed. Noise components attributed to head movement, white matter, cardiac pulsation, arterial, and large vein related contributions were removed using FMRIB's ICA-based X-noiseifier (ICA-FIX) [13]. Time series were mapped to the standard grayordinate space, with a cortical ribbon-constrained volume-to-surface mapping algorithm. The total mean of the time series of each left-to-right/right-to-left phase-encoded data was subtracted to adjust the discontinuity between the two datasets, and these were concatenated to form a single time series data. A functional connectivity matrix was constructed via linear correlations of the fMRI time series of different Desikan-Killiany atlas parcels [5]. Fisher's r-to-z transformations rendered connectivity values more normally distributed [14], and we averaged the connectivity matrices across participants to construct a group-average functional connectome, also available via the ENIGMA Toolbox (https://github.com/MICA-MNI/ENIGMA) [15].

c) MICs data: MICs data were preprocessed using micapipe (https://github.com/MICA-MNI/micapipe), which integrates AFNI, FSL, FreeSurfer, ANTs, and Workbench [2,6,7,16,17].

c-i) T1-weighted data: Data were de-obliqued, reoriented, intensity non-uniformity corrected, and skull stripped. Models of the inner and outer cortical surfaces were generated using FreeSurfer [1–4], and segmentation errors were manually corrected.

c-ii) qT1 data: After registering qT1 data to FreeSurfer space using a boundary-based registration [18], we generated 14 equivolumetric intracortical surfaces and sampled qT1 intensity as *in vivo* proxies of depth-dependent cortical microstructure [12]. The microstructural profile similarity matrix was constructed using the same procedures as for the HCP data.

c-iii) rs-fMRI data: We discarded the first five volumes, removed the skull, and corrected for head motion. Magnetic field inhomogeneity was corrected using topup with reversed phase-encoded data [19]. After applying a high-pass filter at 0.01 Hz, noise components attributed to head movement, white matter, cardiac pulsation, arterial, and large vein related contributions were removed using ICA-FIX [13]. Preprocessed time series were mapped to the standard grayordinate space, with a cortical ribbon-constrained volume-to-surface mapping algorithm. After regressing out time series spikes, a functional connectivity matrix was constructed by calculating linear correlations of time series between different Desikan-Killiany parcels [5]. We applied Fisher's r-to-z transformation to the individual functional connectivity matrix and averaged across participants to construct a group-average functional connectome.

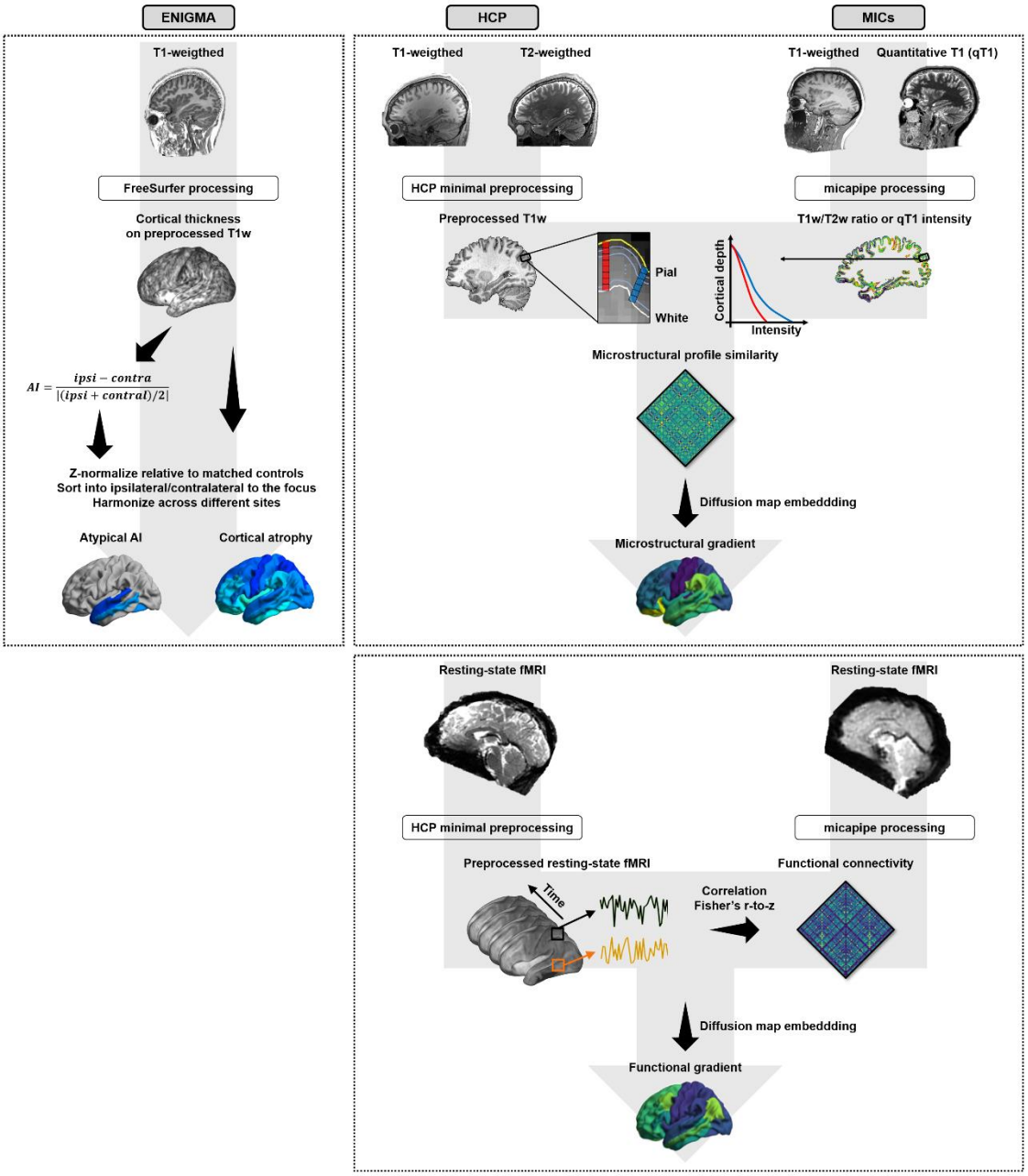

Supplementary Figure 1 Multimodal processing. T1-weighted data from ENIGMA consortium underwent FreeSurfer-based preprocessing and were used for calculating atypical asymmetry and cortical atrophy in TLE patients relative to controls. Structural and functional MRI from the HCP and MICs datasets were preprocessed, and we generated microstructural/functional gradients using non-linear dimensionality reduction techniques. *Abbreviations:* HCP, Human Connectome Project; MICs, microstructure-informed connectomics; AI, asymmetry index; ipsi, ipsilateral; contra, contralateral; fMRI, functional magnetic resonance imaging.

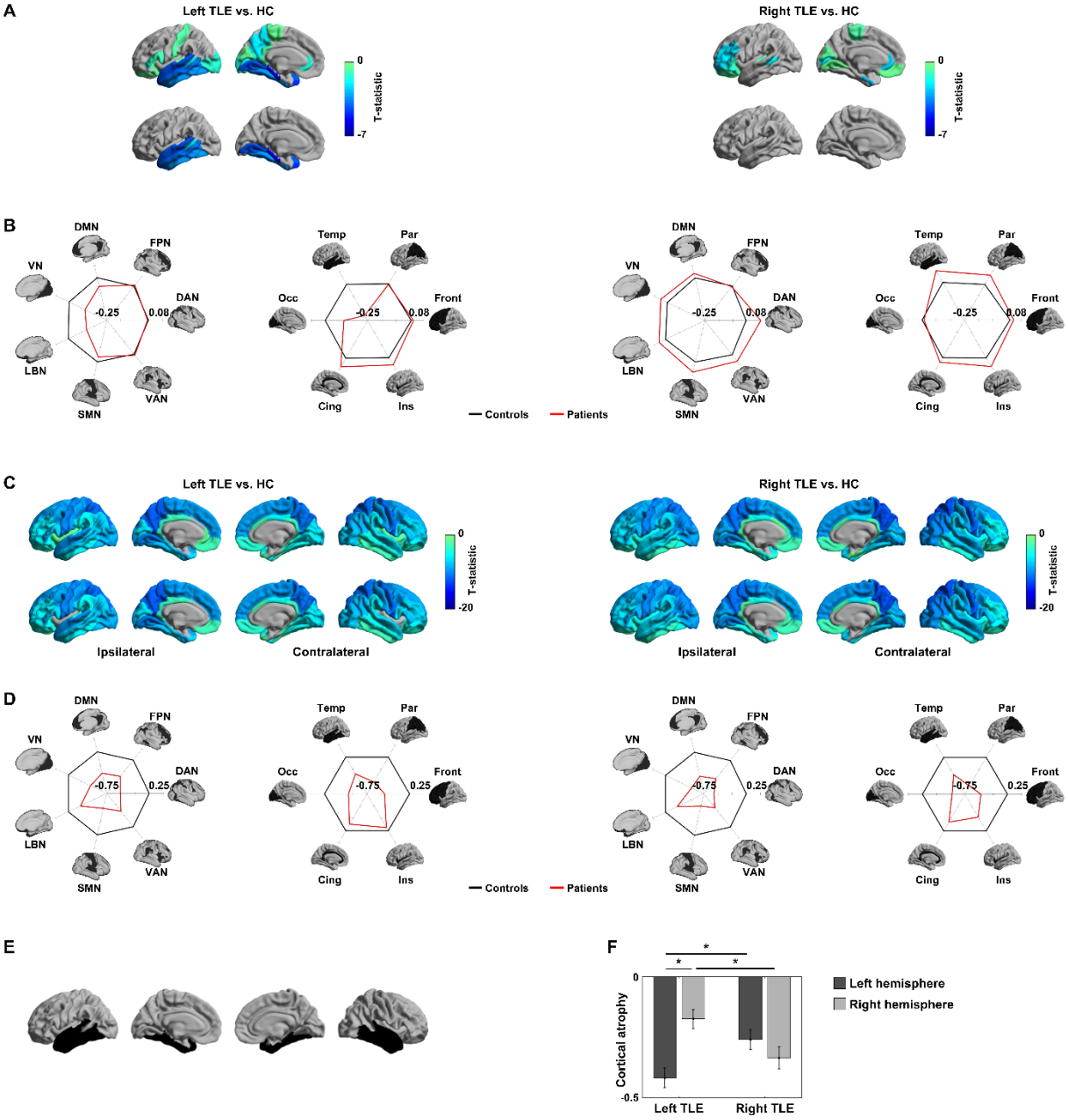

Supplementary Figure 2 Results of left and right TLE. (A) Atypical cortical asymmetry in left and right TLE and **(B)** stratification of the effects (*i.e.*, asymmetry index) according to functional communities and lobes. **(C-D)** Results for cortical atrophy. **(E)** Location of the temporal lobe. **(F)** Cortical atrophy in left and right TLE patients relative to controls for each hemisphere in the temporal lobe. Significant differences are marked with asterisks. For details, see *Fig. 1*.

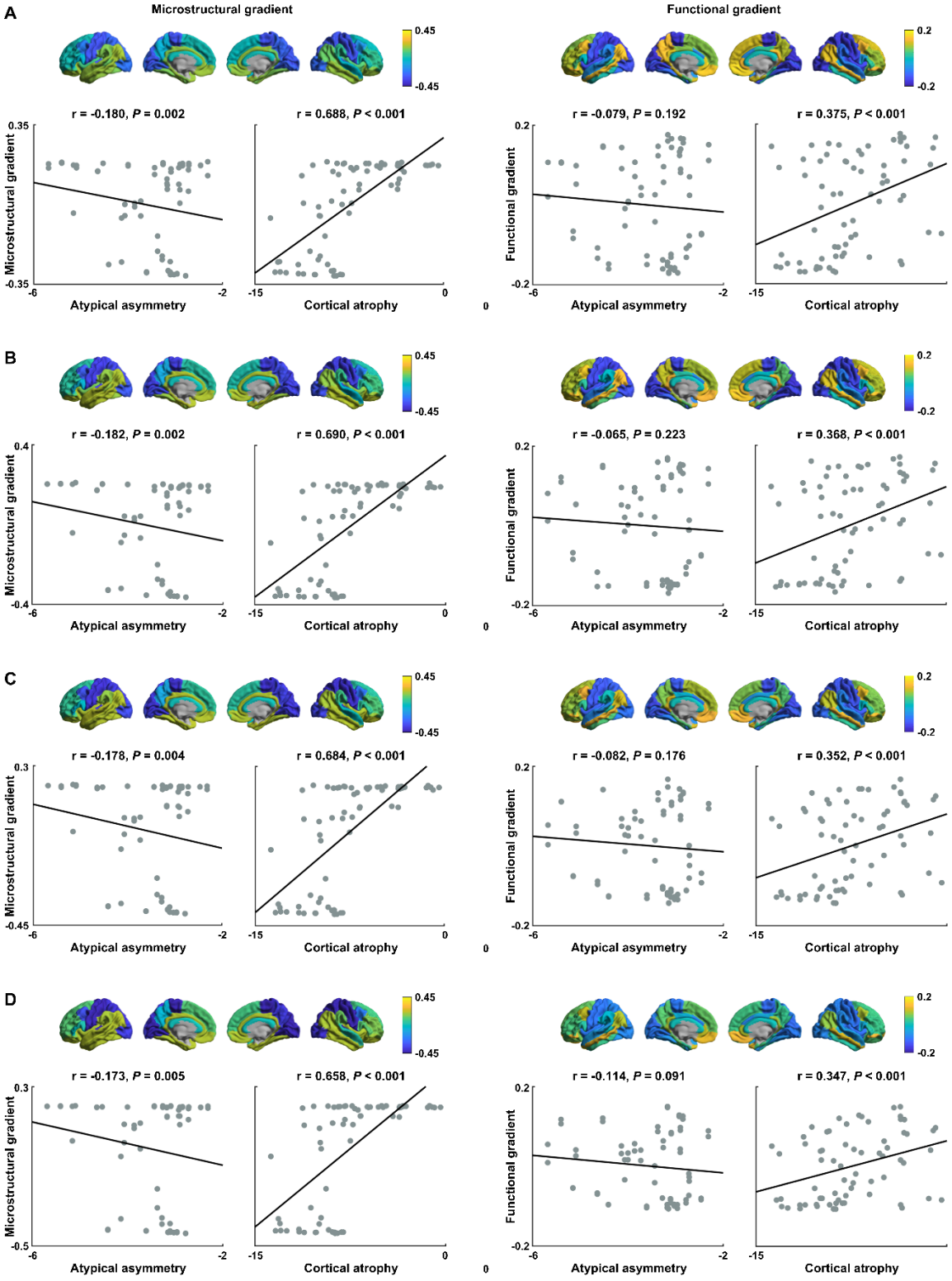

Supplementary Figure 3 Results from different connectome densities. Microstructural and functional gradients derived from **(A)** 20, **(B)** 30, **(C)** 40, and **(D)** 50% density of connectivity matrices. Scatter plots show spatial correlations between microstructural/functional gradients and atypical cortical asymmetry (left) and atrophy (right).

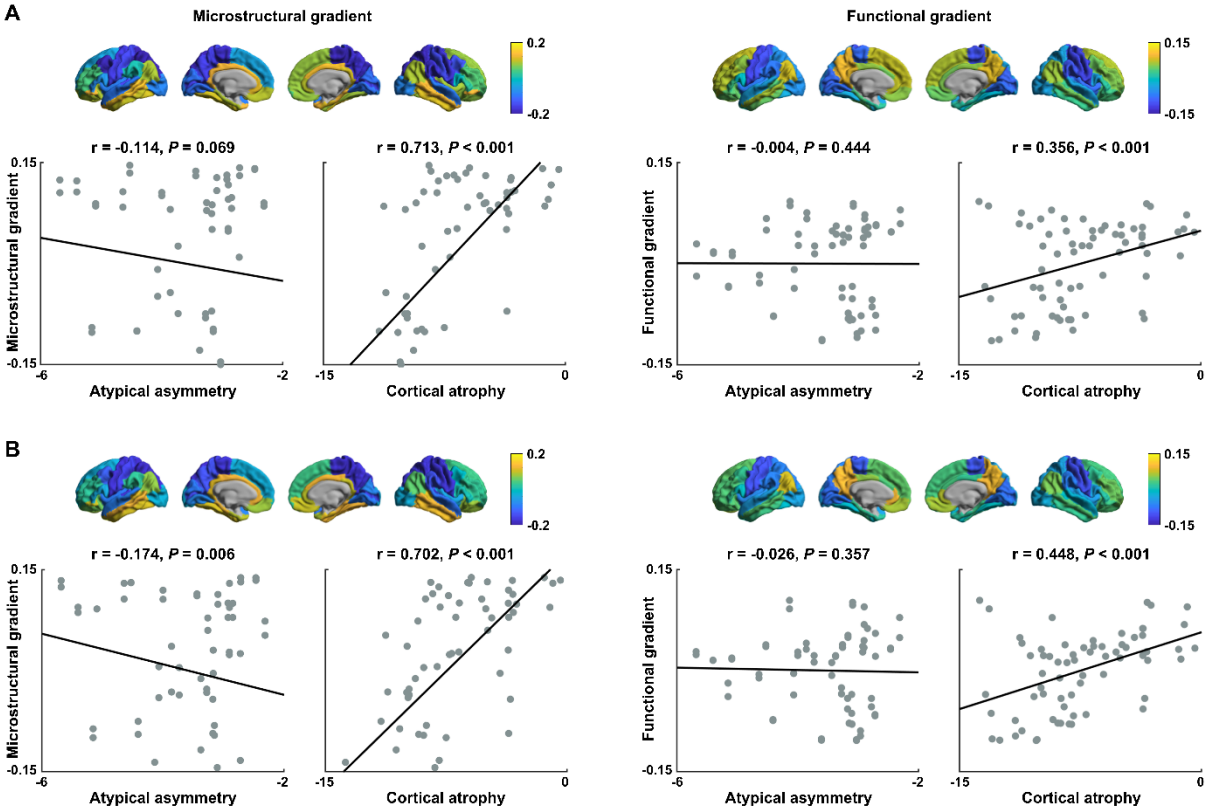

Supplementary Figure 4 Gradients obtained from locally acquired microstructural and functional MRI data in healthy controls and patients with TLE. (A) Microstructural (left) and functional (right) gradients in healthy controls are shown on the brain surface. Associations between atypical cortical asymmetry and atrophy and these gradients are shown in the scatter plots. **(B)** Gradients and associations presented for patients with TLE.

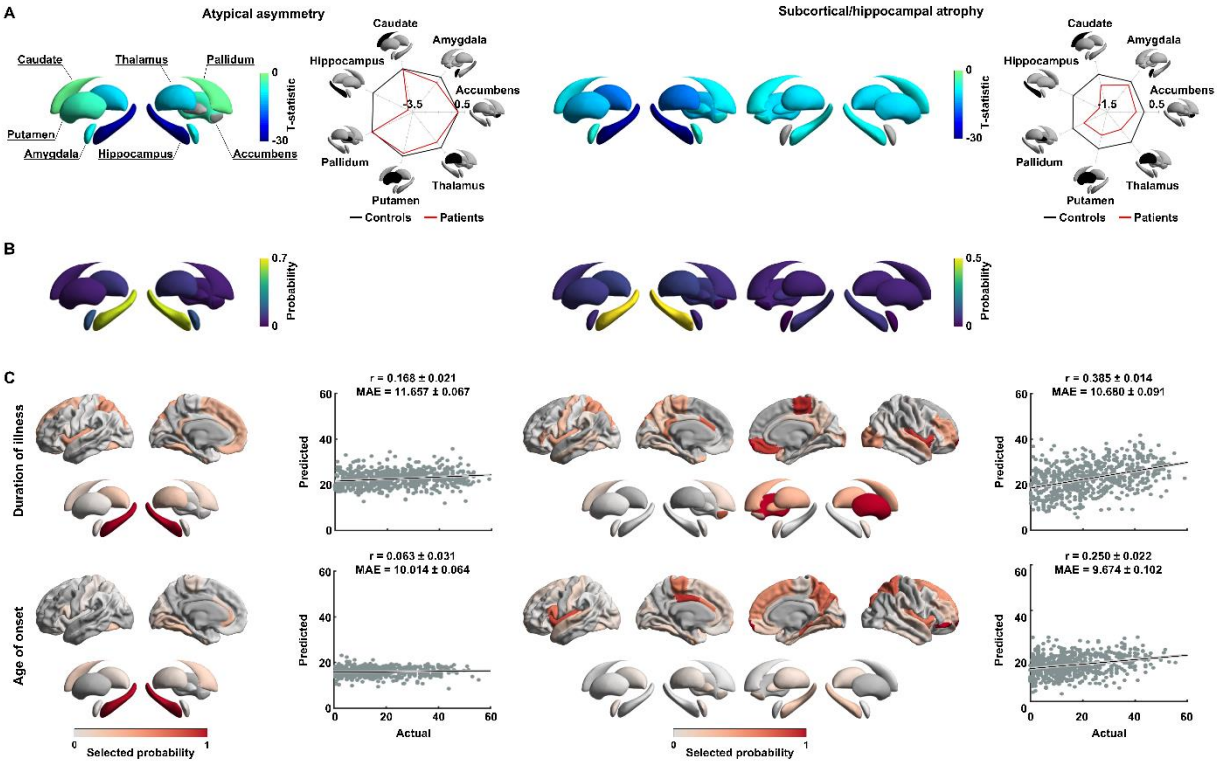

Supplementary Figure 5 Analyses for subcortical and hippocampal volume. (A) Atypical asymmetry of subcortical/hippocampal volume differences and atrophy between individuals with TLE and controls. **(B)** Consistency probability of atypical asymmetry and atrophy in subcortical/hippocampal volume across individuals. **(C)** Prediction results for (top) duration of epiulepsy and (bottom) age at seizure onset using cortical and subcortical features. For details, see *Fig. 1, 2, and 3*.

REFERENCES

1. Dale AM, Fischl B, Sereno MI. Cortical surface-based analysis: I. Segmentation and surface reconstruction. *Neuroimage*. 1999;9(2):179-194. doi:10.1006/nimg.1998.0395
2. Fischl B. FreeSurfer. *Neuroimage*. 2012;62(2):774-781. doi:10.1016/j.neuroimage.2012.01.021
3. Fischl B, Sereno MI, Dale AM. Cortical surface-based analysis: II. Inflation, flattening, and a surface-based coordinate system. *Neuroimage*. 1999;9(2):195-207. doi:10.1006/nimg.1998.0396
4. Fischl B, Sereno MI, Tootell RBH, Dale AM. High-resolution inter-subject averaging and a surface-based coordinate system. *Hum Brain Mapp*. 1999;8:272-284. doi:10.1002/(SICI)1097-0193(1999)8
5. Desikan RS, Ségonne F, Fischl B, et al. An automated labeling system for subdividing the human cerebral cortex on MRI scans into gyral based regions of interest. *Neuroimage*. 2006;31(3):968-980. doi:10.1016/j.neuroimage.2006.01.021
6. Jenkinson M, Beckmann CF, Behrens TEJ, Woolrich MW, Smith SM. Fsl. *Neuroimage*. 2012;62(2):782-790. doi:10.1016/j.neuroimage.2011.09.015
7. Glasser MF, Sotiropoulos SN, Wilson JA, et al. The minimal preprocessing pipelines for the Human Connectome Project. *Neuroimage*. 2013;80:105-124. doi:10.1016/j.neuroimage.2013.04.127
8. Van Essen DC, Glasser MF, Dierker DL, Harwell J, Coalson T. Parcellations and hemispheric asymmetries of human cerebral cortex analyzed on surface-based atlases. *Cereb cortex*. 2012;22(10):2241-2262. doi:10.1093/cercor/bhr291
9. Glasser MF, Coalson TS, Robinson EC, et al. A multi-modal parcellation of human cerebral cortex. *Nature*. 2016;536(7615):171-178. doi:10.1038/nature18933
10. Glasser MF, Goyal MS, Preuss TM, Raichle ME, Van Essen DC. Trends and properties of human cerebral cortex: Correlations with cortical myelin content. *Neuroimage*. 2014;93:165-175. doi:10.1016/j.neuroimage.2013.03.060
11. Glasser MF, Van Essen DC. Mapping human cortical areas in vivo based on myelin content as revealed by T1- and T2-weighted MRI. *J Neurosci*. 2011;31(32):11597-11616. doi:10.1523/JNEUROSCI.2180-11.2011
12. Paquola C, Vos De Wael R, Wagstyl K, et al. Microstructural and functional gradients are increasingly dissociated in transmodal cortices. *PLoS Biol*. 2019;17(5):e3000284. doi:10.1371/journal.pbio.3000284
13. Salimi-Khorshidi G, Douaud G, Beckmann CF, Glasser MF, Griffanti L, Smith SM. Automatic denoising of functional MRI data: Combining independent component analysis and hierarchical fusion of classifiers. *Neuroimage*. 2014;90:449-468. doi:10.1016/j.neuroimage.2013.11.046
14. Thompson WH, Fransson P. On Stabilizing the Variance of Dynamic Functional Brain Connectivity Time Series. *Brain Connect*. 2016;6(10):735-746. doi:10.1089/brain.2016.0454
15. Larivière S, Paquola C, Park B, et al. The ENIGMA Toolbox: multiscale neural contextualization of multisite neuroimaging datasets. *Nat Methods*. Published online June 30, 2021. doi:10.1038/s41592-021-01186-4
16. Cox RW. AFNI : Software for Analysis and Visualization of Functional Magnetic Resonance Neuroimages. *Comput Biomed Res*. 1996;29:162-173. doi:10.1006/cbmr.1996.0014

17. Avants BB, Tustison NJ, Song G, Cook PA, Klein A, Gee JC. A reproducible evaluation of ANTs similarity metric performance in brain image registration. *Neuroimage*. 2011;54(3):2033-2044. doi:10.1016/j.neuroimage.2010.09.025

18. Greve DN, Fischl B. Accurate and robust brain image alignment using boundary-based registration. *Neuroimage*. 2009;48(1):63-72. doi:10.1016/j.neuroimage.2009.06.060

19. Andersson JLR, Skare S, Ashburner J. How to correct susceptibility distortions in spin-echo echo-planar images: Application to diffusion tensor imaging. *Neuroimage*. 2003;20(2):870-888. doi:10.1016/S1053-8119(03)00336-7